Atmospheric
Chemistry
and Physics
Discussions

Open Access

Modeling upper tropospheric and lower stratospheric water vapor anomalies

M. R. Schoeberl[1], A. E. Dessler[2], and T. Wang[2]

[1]Science and Technology Corporation, Lanham, MD, USA
[2]Texas A&M University, College Station, TX, USA

Correspondence to: M. R. Schoeberl (mark.schoeberl@mac.com)

Discussion Paper | Discussion Paper | Discussion Paper | Discussion Paper

ACPD

13, 9653–9679, 2013

Tropospheric and stratospheric water vapor anomalies

M. R. Schoeberl et al.

Title Page

Abstract	Introduction
Conclusions	References
Tables	Figures

|◄ | ►|
◄ | ►
Back | Close

Full Screen / Esc

Printer-friendly Version

Interactive Discussion

Abstract

The domain-filling, forward trajectory calculation model developed by Schoeberl and Dessler (2011) is used to further investigate processes that produce upper tropospheric and lower stratospheric water vapor anomalies. We examine the pathways parcels take from the base of the tropical tropopause layer (TTL) to the lower stratosphere. Most parcels found in the lower stratosphere arise from East Asia, the Tropical West Pacific (TWP) and the Central/South America. The belt of TTL parcel origins is very wide compared to the final dehydration zones near the top of the TTL. This is due to the convergence of rising air as a result of the stronger diabatic heating near the tropopause relative to levels above and below. The observed water vapor anomalies – both wet and dry – correspond to regions where parcels have minimal displacement from their initialization. These minimum displacement regions include the winter TWP and the Asian and American monsoons. To better understand the stratospheric water vapor concentration we introduce the water vapor spectrum and investigate the source of the wettest and driest components of the spectrum. We find that the driest air parcels that originate below the TWP, moving upward to dehydrate in the TWP cold upper troposphere. The wettest air parcels originate at the edges of the TWP as well as the summer American and Asian monsoons. The wet air parcels are important since they skew the mean stratospheric water vapor distribution toward higher values. Both TWP cold temperatures that produce dry parcels as well as extra-TWP processes that control the wet parcels determine stratospheric water vapor.

1 Introduction

A broad understanding of the stratospheric circulation began over 60 yr ago with the publication of Brewer's seminal paper (Brewer, 1949). In order to account for the dryness of the stratosphere, Brewer noted that air must have been entering the stratosphere through the coldest part of the tropopause, found in the tropics. Mass conser-

Title Page

Abstract	Introduction
Conclusions	References
Tables	Figures

|◄ | ►|

◄ | ►

Back | Close

Full Screen / Esc

Printer-friendly Version

Interactive Discussion

vation requires that this tropical upward circulation would have descending branches in the extra-tropics. Newell and Gold-Stewart (1981), again using stratospheric water vapor and tropopause temperature observations, suggested that most of the air reaching the stratosphere was moving upward through the very coldest part of the tropical tropopause, the winter Tropical West Pacific (TWP), a region they termed the "stratospheric fountain." Subsequent measurements of tropospheric trace gases suggest that the winter tropical west Pacific is the primary locus of air entering the stratosphere during Boreal winter. On the other hand satellite observations during boreal summer have identified the summer Asian monsoon as another possible region for tropospheric air to enter the stratosphere (Randel, 2010; Bergman et al., 2013).

Sherwood and Dessler (2000) defined the Tropical Tropopause Layer (TTL), a transition layer between the troposphere and stratosphere to extend from the level of zero net-radiative heating (~ 13–14 km, 355–360 K potential temperature) to the highest level that convection reaches (~ 18–19 km, 380–400 K).

The TTL is sometimes referred to as the "tape-head for the water vapor tape recorder" and, indeed, tape recorder signals gets stronger with altitude through the TTL (Gettleman et al., 2010). The TTL base is the zone of primary convective detrainment although convective detrainment continues above the base of the TTL with decreasing frequency (Dessler, 2002; Zipser, 2006). Convective detrainment is the primary mechanism by which pollutants from the lower troposphere are deposited into the TTL (Fueglistaler et al., 2009). From a Lagrangian perspective, once air parcels reach the TTL, they move upward due to positive net radiative heating rates encountering colder temperature. When parcel relative humidity exceeds some threshold value, ice forms (Jensen et al., 1996) and is gravitationally removed dehydrating the air parcels. Parcel water vapor concentration is primarily determined by the minimum parcel path temperature (e.g. Mote et al., 1996; Holton and Gettelman, 2001; Fueglistaler et al., 2005, 2009; Liu et al., 2010). We refer to the last point on the parcel path that fixes the water vapor concentration as the final dehydration point (FDP) sometimes called the Lagrangian dry point (Liu et al., 2010). As found by Schoeberl and Dessler (2010, here

after SD2010), maps of the FDP distribution show that most parcels complete the dehydration process in the Tropical West Pacific (TWP) as originally theorized by Newell and Gold-Stewart (1981). This does not mean the parcels are "entering stratosphere" in the same region. In fact, the dehydration process and the process of entering the stratosphere are different processes that may occur at different locations as we will show below.

Following the ideas introduced by age-of-air studies (Schoeberl et al., 2000; Waugh and Hall, 2002) we can use this Lagrangian perspective on parcel statistics and dehydration. We define an "air sample" as spatial region containing a number of parcels with different ages and water vapor concentrations. The sample age and water vapor amount is the ensemble average of parcel age and water vapor concentration, respectively. The temperature along the parcel path into the stratosphere determines the parcel's water vapor concentration, and the time it takes to travel the path determines the parcel age. Understanding the preferred pathways into the stratosphere is fundamental to understanding the water vapor concentration as well as age. This information is useful in understanding water vapor as well as understanding how short-lived ozone depleting substances might gain entry into the stratosphere (Levine et al., 2007; Salawitch et al., 2005).

Below (Sect. 2) we first describe the model set up and the observations that motivate this analysis. Section 3 shows the results of our simulations, our estimates of parcel displacement from initial forcing regions, sources of wet and dry air, and we introduce the water vapor spectrum. Section 4 summarizes our research and ends with conclusions.

Printer-friendly Version

Interactive Discussion

2   Model and observations

2.1   Reanalysis data sets and model set up

The results shown in this paper are from the forward domain filling diabatic trajectory model as described in SD2010 and in Schoeberl et al. (2012) (S2012). In this study, we use 6 hourly wind, temperature and heating rate analyses from NASA's Modern-Era Retrospective Analysis for Research and Application (MERRA, Rienecker, et al., 2011), NOAA's Climate Forecast System Reanalysis (CFSR, Saha et al., 2010) and ECMWF's ERA Interim reanalysis (ERAi, Dee et al., 2011) to drive the model. These three reanalyses are described and compared in more detail at http://reanalyses.org/ atmosphere/comparison-table. The diabatic heating rates includes the radiative effects of gases, clouds, turbulent heating, etc.

   Forward domain-filling for this study works as follows: every six hours, corresponding to an analysis time, we use a random number generator to initialize 550 parcels randomly distributed from 0–360° longitude and ± 60° latitude. For each parcel, the initialization level is chosen to be above the zero diabatic heating level, but not lower than 360 K or above the tropopause. Our tropopause is determined from the analyses to be the lowest of the following in an atmospheric profile: the cold point, the $-2\,\mathrm{K\,km^{-1}}$ lapse rate (the WMO definition), or the 380 K surface. This means that in the Asian monsoon region, parcels would be initiated at about 370 K since the level of zero heating is higher there.

   After initialization, the parcels move upward into the stratosphere, filling the stratospheric domain. Generally, parcels move downward at extra tropical latitudes and those moving below 250 hPa are removed – we assume they have re-entered the troposphere. Parcels are initiated with 50 ppmv (parts per million by volume) of water vapor, and we dehydrate parcels to saturation when the relative humidity exceeds a predetermined threshold, e.g. 100 %. We use the saturation over ice temperature – water vapor relationship described in Murphy and Koop (2005). As with most trajectory models of this type we assume that when saturation (or super-saturation) is reached the

excess water vapor is instantly removed and the relative humidity is reduced to 100 %. In addition to water vapor, we carry the methane (CH_4) concentration for each parcel. Methane is oxidized in the stratosphere and the resulting water is added to the parcel, as described in SD2010. Tropospheric methane initial values are increased linearly from 1.54 ppmv in 1979 to 1.8 ppmv in 2010. The oxidation rate of methane is interpolated from a two-dimensional stratospheric chemistry model (Fleming et al., 2007) onto parcel locations.

In a diabatic trajectory model, the net heating rates controls vertical transport. Figure 1 shows the time mean Boreal winter (DJF – December, January, February) and summer (JJA – June, July, August) upper tropical troposphere temperatures and heating rate fields at a log-pressure height of 17 km ($\sim$ 90 hPa). In DJF (Fig. 1a), the strongest heating occurs in the west Pacific region, split across the equator with one zone east of the Philippines and second spread over Australia. Secondary heating zones occur over central and western South America. The strongest cooling zone is co-located with the Aleutian anticyclone (Boville, 1960). All three analyses show that the coldest upper tropospheric tropical temperatures are roughly co-located with the peaks in heating.

In contrast to DJF, JJA (Fig. 1b) shows the strongest heating over the Asian monsoon region extending to the Near East through the Mediterranean, but overall less heating than in DJF. Smaller heating regions are present east of Central America and northern Australia. The coldest time mean summer TTL temperatures are over the Asian monsoon at about $\sim$ 193 K, but in winter the coldest time-mean TWP temperature is $\sim$ 188 K. The ice saturation mixing ratio difference for these two temperatures is almost 2.5 ppmv given the same pressure level. The zonal mean heating rate for summer and winter (Fig. 1c, d, respectively) shows that the heating rate is much stronger in winter over a broader latitudinal extent than in summer. The black dots in Fig. 1c, d illustrate the model's zonal mean initialization level.

2.2 Observations

Most of our comparisons will be with the 2005 to 2010 Aura Microwave Limb Sounder (MLS) measurements (Read et al., 2007) made between 2005 and 2010. In S2012 we showed that MERRA and CFSR are in good agreement with Singapore sondes, with ERAi being cold biased. Even a small bias in reanalysis temperatures can produce a significant shift in water vapor concentration (e.g. Randel et al., 2004; SD2012) and we see this in our model simulations – ERAi's stratosphere is relatively dry compared to observations and the other models.

While the model can include simple parameterization for the effects of gravity waves and convection, as well as allowing for super-saturation (see SD2010), for these experiments we turn off all the parameterizations and assume that water is instantly removed at 100 % saturation. Including these additional processes does not affect our results.

3 Water vapor simulations

Before we explore the various pathways that lead to anomalies it is useful to verify the quality of the simulations as compared to MLS observations. Figure 2 shows the water vapor patterns at 100 and 83 hPa ($\sim$ 16 and $\sim$ 17.5 km) from the five-year winter (DJF) and summer (JJA) averages for the MLS and the three reanalyses discussed in S2012 and above. The fields are adjusted so that the model zonal mean is the same as the MLS zonal mean. First, we note that the three summer and winter reanalyses water vapor distributions are broadly consistent with MLS and with each other. During DJF, the lowest mixing ratios occur over the TWP with minor dry features over Africa and Central/South America at 100 hPa. Higher up, the TWP low water vapor feature has spread across the tropics to the Indian Ocean and Africa. The bands of high water vapor at higher latitudes are due to methane-enhanced water vapor descending from the mid-stratosphere.

Title Page

Abstract | Introduction

Conclusions | References

Tables | Figures

|◀ | ▶|

◀ | ▶

Back | Close

Full Screen / Esc

Printer-friendly Version

Interactive Discussion

The summer (JJA) 100 hPa model fields show water vapor enhancements over the Asian monsoon and Central/South America associated with monsoonal circulations. The models also show a broad dry feature over the Indian Ocean that extends into the West Pacific. This dry feature is not as evident in MLS data; MLS observes the feature further east. At 83 hPa the water vapor feature over the Asian monsoon has enlarged while the Central/South American feature is weaker. The Indian Ocean tropical dry feature has vanished. The Asian monsoon wet anomaly extends into the near east, and follows the heating zone shown in Fig. 1b.

The good agreement between the MLS water vapor features and the model features give us confidence that the models can be used to further understand water vapor anomalies in the upper troposphere. It is also somewhat surprising. Dessler and Sherwood (2004) argued that the monsoonal high water vapor features are related to convection. Our model, however, does not include convective moistening, so this indicates that a model including only slow radiative ascent can also accurately simulate these features.

3.1 Parcel displacement in the TTL

Holton and Gettelman (2001) noted that parcels moving upward from the lower TTL into the stratosphere might travel long horizontal distances within the TTL. Fueglistaler et al. (2004) (hereafter F2004) trajectory calculations showed that the distances traveled could be tens of thousand of kilometers between 350 K and the dehydration point.

Following the approach of F2004 we can compute the distance between the parcel initiation and the point at which a parcel crosses the 370 K and 380 K surfaces – we refer to this distance as the displacement. The 370 K surface is close to the coldest region of the tropopause and thus roughly the FDP, and the 380 K surface is approximately the base of the stratosphere in the tropics. In Fig. 3 we show the gridded average displacement initialized parcels move before they cross the 370 K and 380 K surfaces for winter and summer seasons.

For winter the plots (Fig. 3a, b) show that very little displacement of parcels from $360 \rightarrow 370$ K over a region stretching from the Africa to the TWP, and South America. Above 370 K the displacement is larger especially over the Eastern Pacific. The TWP upper troposphere consists of a cold pool dominated by a high pressure system (required by hydrostatic balance) in which air circulates around producing little displacement. The strong diabatic heating in the TWP moves the air parcels rapidly up through this region. North of the TWP the westerly subtropical jet moves parcels rapidly producing a large displacement. East of the TWP a similar high pressure system also develops over the South American cold pool. The polar jet dips equatorward between the TWP and South American system creating a high displacement zone in the East Pacific. The lowest displacement features – centered on the cold pools – correspond to the lowest winter water vapor anomalies shown in Fig. 2.

During summer the tropical Pacific winds are weaker and the air ascends to 370 K and 380 K without much displacement. In contrast to winter, the lowest displacement features correspond to high water vapor features seen in Fig. 2. The summer high pressure system over the Asian monsoon region shows low displacement, and this low displacement feature extends up through 370 K to 380 K. Bergman et al. (2013) has noted the almost complete isolation of the air within the Asian monsoon high pressure system; their back trajectories initiated within the upper troposphere anticyclone descend almost vertically to the surface. The high water vapor anomaly over Central/South America also corresponds to a low displacement region but this displacement feature is not as dramatic at 380 K.

The colocation of low displacement features and water vapor anomalies makes sense in that low displacement regions are isolated so that their water vapor signatures, either high or low, appear because there is less mixing with surrounding air.

3.2 Water vapor spectrum

In order to further understand how water vapor is controlled within the stratosphere we introduce the water vapor spectrum. As discussed above, the water vapor spectrum

Title Page

Abstract | Introduction

Conclusions | References

Tables | Figures

◄ | ►►

◄ | ►

Back | Close

Full Screen / Esc

Printer-friendly Version

Interactive Discussion

is analogous to the age-spectrum (Waugh and Hall, 2002) – it is the probability distribution function (PDF) of water vapor concentration of stratospheric parcels. Figure 4 shows the stratospheric water vapor spectrum for the three reanalyses. All parcels above 380 K are considered, and water from methane oxidation is not included. The distribution shown in Fig. 4 is fairly broad with values ranging from 0.5 to 9 ppmv and skewed toward higher values in all three cases. The skewed distribution weights the mean toward a higher concentration than the mode (distribution peak). This means that the wetter air parcels are driving stratospheric water vapor distribution away from the most frequently observed parcels – which, as noted below, come through the TWP region.

The overall ERAi dry bias is evident in Fig. 4, although the shape of the distribution is basically the same. Given the similarity in the distributions and water vapor anomaly fields, we will focus on MERRA for the rest of the paper. Figure 5 shows a two-dimensional histogram of the MERRA water-vapor spectrum vs. age (the time since the parcel was initialized). The oscillation of the water vapor field as a function of season is evident and consistent with warmer tropopause temperatures in summer vs. winter. This figure is basically the water vapor tape recorder without mixing (Mote et al., 1986). Figure 6 shows the distribution of parcel initialization locations vs. water vapor amount in the stratosphere for all seasons. We only consider parcels that are above 380 K. Figure 6a shows that the wettest parcels originate at relatively higher latitudes with the mean concentration nearly symmetric around a point just north of the equator. This is consistent with the temperature distributions in Fig. 1, showing that the region with highest temperature and net positive heating are at the edge of the tropics.

Figure 6b shows the longitude distribution and it reveals two major source regions – the TWP and the Americas. These source regions are generally of higher heating rates (Fig. 1). There is also a faint signature of Africa as a minor source region.

Tropospheric and stratospheric water vapor anomalies

M. R. Schoeberl et al.

Full Screen / Esc

Printer-friendly Version

Interactive Discussion

3.3 Transport patterns

F2004 showed that transport through the tropical west Pacific dominated transport from the troposphere to the stratosphere compared to other regions. Our calculations show similar results. Figure 7a shows the spatial density distribution of parcels originating at ∼ 360 K that end up in the stratosphere. This map can be visually compared to the final dehydration map (Fig. 7b). Overall the two maps are similar; there is a spatial correlation of ∼ 0.7 between the origin map and the dehydration map. We agree with F2004 that most of the air moving into the stratosphere is from the TWP, and we find that South America and Africa are significant source regions. The density of FDPs reflects the source regions (Fig. 7a). The major difference between the two maps is that more parcels are originating on the edge of the tropics than one would assume simply by looking at the FDP plot. This means that there is a wider zone for pollutants to enter the stratosphere than might be assumed from the FDP pattern alone.

Figure 7c shows the mixing ratio of water vapor at the final dehydration points that can be compared to F2004 Fig. 4. Figure 7c shows that the wettest parcels are arriving from the edges of the tropics and the longitudes outside of the TWP, which F2004 noted as well. The map confirms the results in Fig. 6a. As an aside, Fig. 7c shows the effect of polar dehydration. Antarctic dehydration yields significantly lower water vapor concentrations than Arctic dehydration; however, neither region has a strong impact on the overall dryness of the stratosphere except that the Southern Hemisphere is slightly drier than the Northern Hemisphere as observed by the MLS (SD2010). As a reference, we show in Fig. 7d the 17 km annual average heating rate and temperatures (similar to Fig. 1 but annual average). The strongest heating is in the TWP in zones north and south of the equator. The location of these ascent regions convolved with the temperature field gives rise to the FDP picture (Fig. 7b).

Figure 8 shows the seasonal dependency of the origin of parcels that reach the stratosphere. During winter (DJF) the dominant region is the equatorial west Pacific and Indian Ocean region. During the summer period, the parcel sources are predom-

Title Page

Abstract | Introduction

Conclusions | References

Tables | Figures

|◄ | ►|

◄ | ►

Back | Close

Full Screen / Esc

Printer-friendly Version

Interactive Discussion

inately over the West Pacific and the ITCZ belt across the Pacific and Atlantic. Somewhat surprisingly, the Indian and North American monsoons do not appear as dominant features – even with strong heating in the monsoon regions (Fig. 1), the monsoons do not appear to be major pathways into the stratosphere despite their distinct appearance in 100 hPa water vapor maps (Fig. 2) and in the displacement map (Fig. 3). The large positive heating rates over monsoon region drives parcels strongly upward, but because of the smaller area of this region, the monsoons are not as important as an origin regions compared to the deeper tropics. ERAi and CFSR show similar results compared to MERRA.

The reason that the tropical belt of parcel sources is so broad compared to the density of FDP points is that the strong heating at the tropopause accelerates the air upward and forces convergence below and divergence above the tropopause. Thus parcels well outside the location of the tropopause cold pools can be drawn into their stronger heating region near the equator – over the TWP or Central America or the Asian summer monsoon. This means it is possible that pollution detrained by convection or rising into the lower half of the TTL, but outside the TWP or other entry zones, can move into the stratosphere, as noted by Hosking et al. (2012).

3.4 Sources of wet and dry parcels

It is evident from the water vapor distributions (Fig. 2) that the wettest and driest parcels are experiencing different temperature histories as well. From Figs. 6a and 7c and as noted above, the wettest parcels appear to originate at the edge of the tropics and in the low displacement zones associated with the monsoon (Fig. 3) while the driest parcels arise near winter TWP. Maps of where the wettest and driest parcels originate at 360 K (Fig. 9) bear this supposition out. The driest parcels originate deep within the tropics whereas the wettest parcels are more dispersed. Evidence of the monsoon influence appears in Fig. 9b with enhancements over India and Central America. Over India, the monsoon anticyclone in the upper troposphere pulls parcels from southern India around the anticyclone into the cold pool (Fig. 1b) where final dehydration occurs

Title Page

Abstract | Introduction

Conclusions | References

Tables | Figures

|◀ | ▶|

◀ | ▶

Back | Close

Full Screen / Esc

Printer-friendly Version

Interactive Discussion

(Fig. 9d). In this region and over Central America, the tropopause is warmer than the TWP by ~ 5 K so parcels that enter into the boreal summer stratosphere will experience relatively less dehydration and produce the water vapor anomalies shown in Fig. 2 (bottom) as we have already noted.

4 Summary and conclusions

Using the forward domain filling trajectory model (SD2010 and S2012) we have investigated the processes that produce anomalies in the water vapor field. Our trajectory parcel statistics allow us to calculate the water vapor spectrum (analogous to the age-spectrum – a PDF of water vapor concentration, Fig. 4), which shows strong seasonal variations (Fig. 5) due to the variations in tropopause temperature – the process that produces the water vapor tape recorder. The spectrum can be linked to pathways parcels take into the stratosphere. Maps of where (~ 360 K) most stratospheric air parcels originate show that instead of a very localized entry zone in the West Pacific, as might be assumed from the final dehydration maps, parcels entering the stratosphere originate from broad tropical regions. Driest air parcels originate in the core of the TWP whereas the wettest parcels originate at the edges of the TWP and South America in winter as well as the monsoons in summer. These results are similar to the findings of F2004. We call the distance that parcels move from their initialization point the displacement. Displacement from initialization to 370 K and 380 K show regional preferences of parcels with little movements. These include the winter TWP and summer Asian and American monsoon. The low displacement regions correspond to locations of high and low water vapor anomalies. The anomalies occur because air is isolated in the low displacement zones.

Figure 10 summarizes the view of winter air parcel processing implied by our results. The strong heating near the tropopause causes air to converge into the cold TWP region with divergence in the stratosphere above. Compared with the parcels at the tropical cold core, parcels at the edge of the tropical core experience warmer

Title Page

Abstract | Introduction

Conclusions | References

Tables | Figures

◄ | ►

◄ | ►

Back | Close

Full Screen / Esc

Printer-friendly Version

Interactive Discussion

temperatures and weaker heating rates. Fewer of these less dehydrated parcels enter the stratosphere, but they skew the water vapor spectrum toward higher mean values. Along the equator, the TWP local maximum in the heating rate causes more parcels to preferentially ascend in the TWP where temperatures are colder, thus the predom-
5 inance of FDPs near the TWP cold core. However, since the heating rate is positive throughout the tropics, parcels can still ascend into the stratosphere outside the TWP region leading to the population of wetter parcels ascending over South America, for example.

Our results suggest that it is important to understand what controls both the wet
10 and dry parcels. Obviously a decrease in TWP temperatures would shift the stratospheric water vapor concentration lower, while an increase in wet parcel concentration – parcels that enter the stratosphere outside of the TWP – would have a significant effect in increasing stratospheric water. Central and South America consistently appear as zones of entry for wetter air parcels.
15 The understanding that there are a variety of zones from which parcels move into the stratosphere even with mixing ratios well above the mean (see Fig. 3) suggests that there are more opportunities for polluted air to enter the stratosphere than just the TWP or the Asian monsoon region.

References

Bergman, J. W., Fierli, F., Jensen, E., Honomicht, S, and Pan, L.: Boundary layer sources for the Asian anticyclone: regional contributions to a vertical conduit, J. Geophys. Res., 118, 1–16, doi:10.1002/jgrd.50142, 2013.
25 Boville, B. W.: The aleutian stratospheric anticyclone. J. Meteorol., 17, 329–336, 1960.
Corti, T., Luo, B. P., Fu, Q., Vömel, H., and Peter, T.: The impact of cirrus clouds on tropical troposphere-to-stratosphere transport, Atmos. Chem. Phys., 6, 2539–2547, doi:10.5194/acp-6-2539-2006, 2006.

Dee, D. P. and coauthors: The ERA-Interim reanalysis: configuration and performance of the data assimilation system, Q. J. Roy. Meteor. Soc., 137, 553–597, 2011.

Dessler, A. E.: The effect of deep, tropical convection on the tropical tropopause layer, J. Geophys. Res., 107, 4033, doi:10.1029/2001JD000511, 2002.

Dessler, A. E. and Sherwood, S. C.: The effect of convection on the summertime extratropical lower stratosphere, J. Geophys. Res., 109, D23301, doi:10.1029/2004JD005209, 2004.

Fleming, E. L., Jackman, C. H., Weisenstein, D. K., and Ko, M.: The impact of inter-annual variability on multi-decadal total ozone simulations, J. Geophys. Res., 112, D10310, doi:10.1029/2006JD007953, 2007.

Folkins, I. and Martin, R. V.: The vertical structure of tropical convection, and its impact on the budgets of water vapor and ozone, J. Atmos. Sci., 62, 1560–1573, 2005.

Fueglistaler, S., Wernli, H., and Peter, T.: Tropical troposphere-to-stratospheretransport inferred from trajectory calculations, J. Geophys. Res., 109, D03108, doi:10.1029/2003JD004069, 2004.

Fueglistaler, S., Bonazzola, M., Haynes, P. H., and Peter, T.: Stratospheric water vapor predicted from the Lagrangian temperature history of air entering the stratosphere in the tropics, J. Geophys. Res., 110, D08107, doi:10.1029/2004JD005516, 2005.

Fueglistaler, S., Dessler, A. E., Dunkerton, T. J., Folkins, I., Fu, Q., and Mote, P. W.: The tropical tropopause layer, Rev. Geophys., 47, RG1004, doi:10.1029/2008RG000267, 2009.

Gettelman, A. and Forster, P. M. F.: A climatology of the tropical tropopause layer, J. Meteorol. Soc. Jpn., 80, 911–924, 2002.

Gettelman, A. and co authors: Multimodel assessment of the upper troposphere and lower stratosphere: tropics and global trends, J. Geophys. Res., 115, D00M08, doi:10.1029/2009JD013638, 2010.

Highwood, E. J. and Hoskins, B. J.: The tropical tropopause, Q. J. Roy. Meteor. Soc., 124, 1579–1604, 1998.

Holton, J. R. and Gettelman, A.: Horizontal transport and dehydration in the stratosphere, Geophys. Res. Lett., 28, 2799–2802, 2001.

Holton, J. R., Haynes, P. H., McIntyre, M. E., Douglass, A. R., Rood, R. B., and Pfister, L.: Stratosphere-troposphere exchange, Rev. Geophys., 33, 403–439, 1995.

Hosking, J. S., Russo, M. R., Braesicke, P., and Pyle, J. A.: Tropical convective transport and the Walker circulation, Atmos. Chem. Phys., 12, 9791–9797, doi:10.5194/acp-12-9791-2012, 2012.

Discussion Paper | Discussion Paper | Discussion Paper | Discussion Paper

Jensen, E. J. and Pfister, L.: Transport and freeze-drying in the tropical tropopause layer, J. Geophys. Res., 109, D02207, doi:10.1029/2003JD004022, 2004.

Jensen E. J., Toon, O. B., Pfister, L., Selkirk, H. B.: Dehydration of the upper troposphere and lower stratosphere by subvisible cirrus clouds near the tropical tropopause, Geophys. Res. Lett., 23, 835–838, 1996.

Levine, J. G., Braesicke, P., Harris, N., Savage, N., and Pyle, J. A.: Pathways and timescales for troposphere-to-stratosphere transport via the tropical tropopause layer and their relevance for very short lived substances, J. Geophys. Res., 112, 1–15, doi:10.1029/2005JD006940, 2007.

Liu, Y. S., Fueglistaler, S., and Haynes, P.: Advection-condensation paradigm for stratospheric water vapor, J. Geophysical Res., 115, D24307, doi:10.1029/2010JD014352, 2010.

Mote, P. W., Rosenlof, K. H., McIntyre, M. E., Carr, E. S., Gille, J. C., Holton, J. R., Kinnersley, J. S., Pumphrey, H. C., Russell III, J. M., and Waters, J. W.: An atmospheric tape recorder: the imprint of tropical tropopause temperatures on stratospheric water vapor, J. Geophys. Res., 101, 3989–4006, 1996.

Murphy, D. M. and Koop, T.: Review of the vapour pressures of ice and supercooled water for atmospheric applications, Q. J. Roy. Meteor. Soc., 131, 1539–1565, 2005.

Newell, R. E., Gould-Stewart, S.: A stratospheric fountain?, J. Atmos. Sci., 38, 2789–2796, 1981.

Read, W. G. and coauthors: Aura microwave limb sounder upper tropospheric and lower stratospheric H_2O and relative humidity with respect to ice validation, J. Geophys. Res., 112, D24S35, doi:10.1029/2007JD008752, 2007.

Quack, B. and Wallace, D. W. R.: Air-sea flux of bromoform: controls, rates, and implications, Global Biogeochem. Cy., 17, 1023, doi:10.1029/2002GB001890, 2003.

Randel, W. J., Fei, W., Oltmans, S. J., Rosenlof, K., Nedoluha, G.: Interannual changes of stratospheric water vapor and correlations with tropical tropopause temperatures, J. Atmos. Sci., 61, 2133–2148, 2004.

Randel, W. J., Park, M., Emmons, L., Kinnison, D., Bernath,, P., Walker, K. A., Boone, C., Pumphrey, H.: Asian monsoon transport of pollution to the stratosphere, Science, 328, 611–613, doi:10.1126/science.1182274,2010.

Rienecker, M. and co-authors: MERRA: NASA's modern-era retrospective analysis for research and applications, J. Climate, 24, 3624–3648, doi:10.1175/JCLI-D-11-00015.1, 2011.

Saha, S. and co-authors: The NCEP climate forecast system reanalysis, B. Am. Meteorol. Soc., 91, 1015–1057, 2010.

Salawitch, R. J., Weisenstein, D. K., Kovalenko, L. J., Sioris, C. E., Wennberg, P. O., Chance, K., Ko, M. K. W., and Mclinden, C. A.: Sensitivity of ozone to bromine in the lower stratosphere, Geophys. Res. Lett., 32, L05811, doi:10.1029/2004GL021504, 2005.

Schiller, C., Grooß, J.-U., Konopka, P., Plöger, F., Silva dos Santos, F. H., and Spelten, N.: Hydration and dehydration at the tropical tropopause, Atmos. Chem. Phys., 9, 9647–9660, doi:10.5194/acp-9-9647-2009, 2009.

Schoeberl, M. R., Sparling, L., Jackman, C., and Fleming, E.: A Lagrangian view of strato-spheric trace gas distributions, J. Geophys. Res., 105, 1537–1552, 2000.

Schoeberl, M. R. and Dessler, A. E.: Dehydration of the stratosphere, Atmos. Chem. Phys., 11, 8433–8446, doi:10.5194/acp-11-8433-2011, 2011.

Schoeberl, M. R., Dessler, A. E., and Wang, T.: Simulation of stratospheric water vapor and trends using three reanalyses, Atmos. Chem. Phys., 12, 6475–6487, doi:10.5194/acp-12-6475-2012, 2012.

Waugh, D. W. and Hall, T. M.: Age of stratospheric air: theory, observations, and models, Rev. Geophys., 40, 1010, doi:10.1029/2000RG000101, 2002.

Zipser, E. J., Cecil, D. J., Liu, C., Nesbitt, S. W., and Yorty, D. P.: Where are the most intense thunderstorms on Earth?, B. Am. Meteorol. Soc., 87, 1057–1071, 2006.

Title Page

Abstract | Introduction

Conclusions | References

Tables | Figures

|◄ | ►|

◄ | ►

Back | Close

Full Screen / Esc

Printer-friendly Version

Interactive Discussion
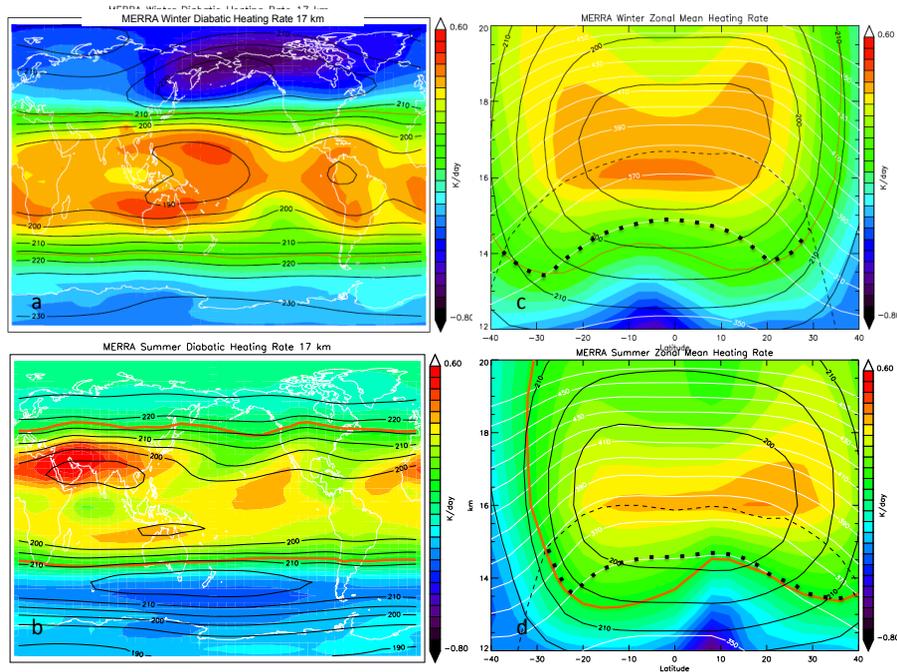
Fig. 1. Heating rates and temperatures from MERRA averaged from 1979–2010. **(a)** 17 km map of heating rates for Boreal winter (DJF) with temperatures (black contours). Thin orange line is the zero heating contour; **(b)** summer (JJA). **(c)** The zonal mean heating rate and temperatures (black contours) and potential temperatures (white). Dashed line shows the zonal mean tropopause. Black dots illustrate the parcel forcing position used in the model; **(d)** summer. The color scheme shows high values in red, low values in blue with the color bar next to each figure indicating the range.
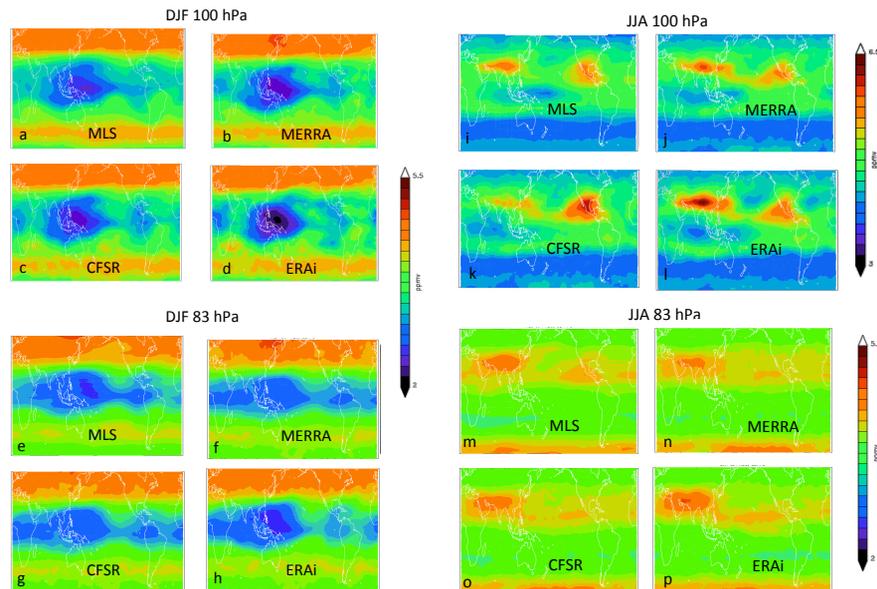
Fig. 2. Water vapor fields for winter at 100 hPa **(a–d)** and at **(e–h)**; and summer 100 hPa **(i–l)** and 83 hPa **(m–p)**. The plots show 2005–2010 five year averages of MLS and the models using the reanalyses indicated in each of the panels. The zonal mean water vapor fields are normalized to the zonal mean MLS field shown in the upper left of each quad-plot. The color scheme and color bars referenced as in Fig. 1.

Winter (DJF)

Summer (JJA)
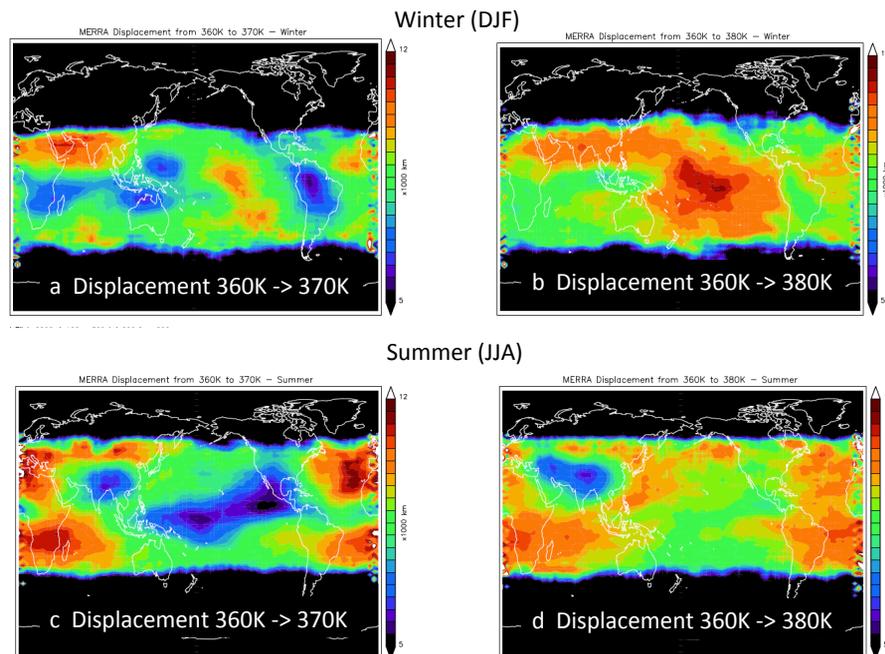
Fig. 3. The average displacement for parcels originating at ~ 360 K reaching the 370 K and 380 K levels. **(a)** DJF for 360 –> 370 K; **(b)** DJF for 360 –> 380 K; **(c)** JJA for 360 –> 370 K, and **(d)** JJA for 360 –> 380 K. Displacement distances range from 5 to 12 thousand km. The color scheme and color bars referenced as in Fig. 1.

Title Page

Abstract | Introduction

Conclusions | References

Tables | Figures

Back | Close

Full Screen / Esc

Printer-friendly Version

Interactive Discussion
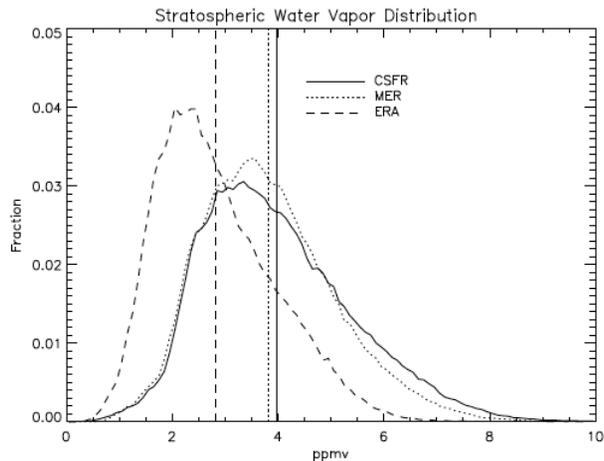
Fig. 4. PDF of water vapor concentration for parcels in the stratosphere. The PDF distribution is normalized by the total number of stratospheric parcels, bin size is 0.1 ppmv. The vertical lines indicate the mean value. ERAi is systematically drier and noted in S2012. Solid lines, CFSR; dotted lines, MERRA, and the dashed line ERAi (labeled ERA in figure).

Title Page

Abstract | Introduction

Conclusions | References

Tables | Figures

|◄ | ►|

◄ | ►

Back | Close

Full Screen / Esc

Printer-friendly Version

Interactive Discussion

Full Screen / Esc

Printer-friendly Version

Interactive Discussion
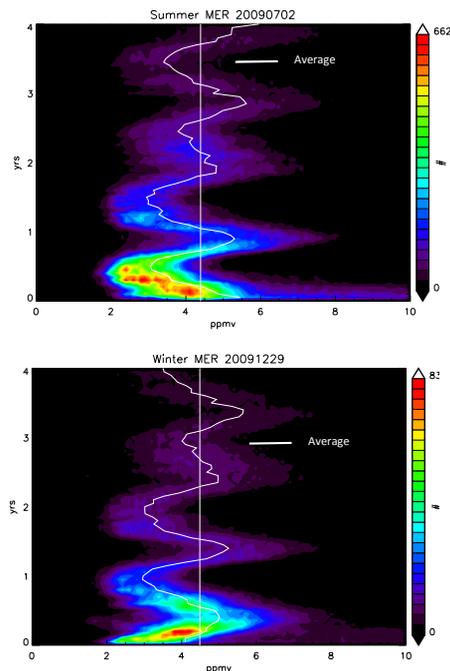
Fig. 5. Water vapor histogram using parcel age vs. water amount for the entire model domain above 18 km. The seasonal oscillation in water vapor distribution is clearly seen. As parcels age they may exit the stratosphere leading fewer parcels in the upper part of the plot. Units number of parcels per bin, 0.1 ppmv bin size for water; 0.05 yr bin size for age. The color scheme and color bars referenced as in Fig. 1.
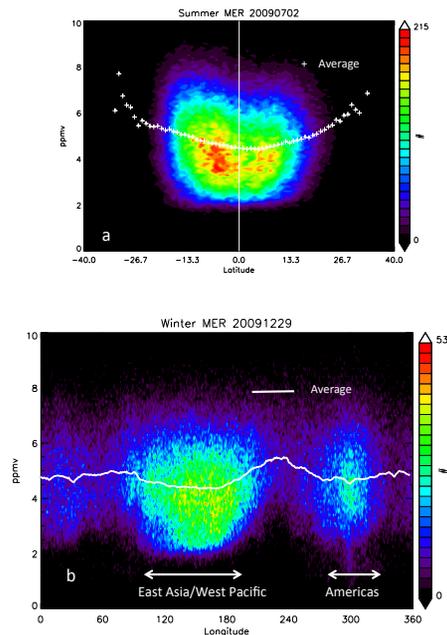
Fig. 6. Joint PDF of MERRA starting locations of parcels that ascended into the stratosphere vs. water vapor. Top, latitude vs. water vapor; bottom, longitude vs. water vapor. The color scheme and color bars referenced as in Fig. 1.
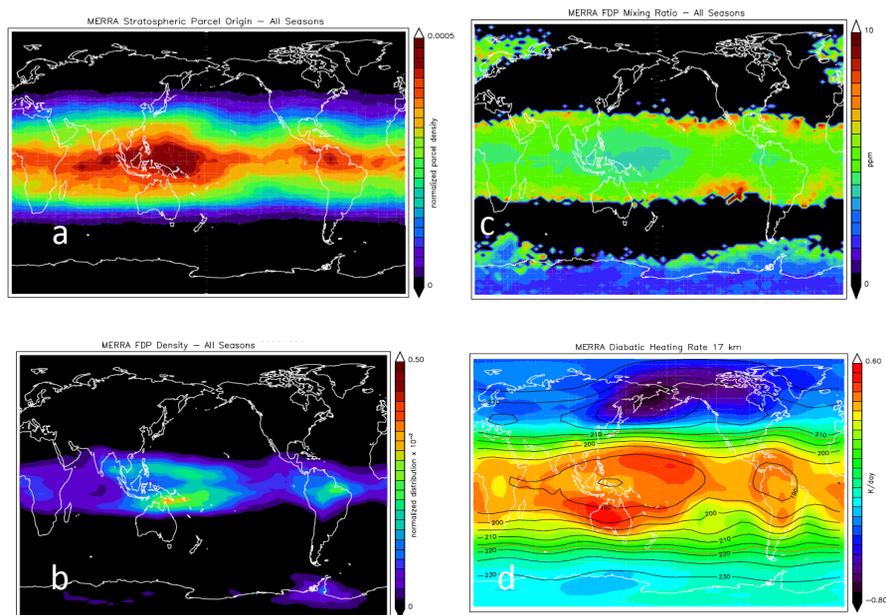
Fig. 7. Statistical results for parcels that end up in the stratosphere. **(a)** Density of origin points at the 360 K level. **(b)** Density of final dehydration locations. **(c)** The average mixing ratio at the final dehydration point in ppm. **(d)** Annual average heating rate at 17 km in K day^{-1} (as in Fig. 1). The color scheme and color bars referenced as in Fig. 1.
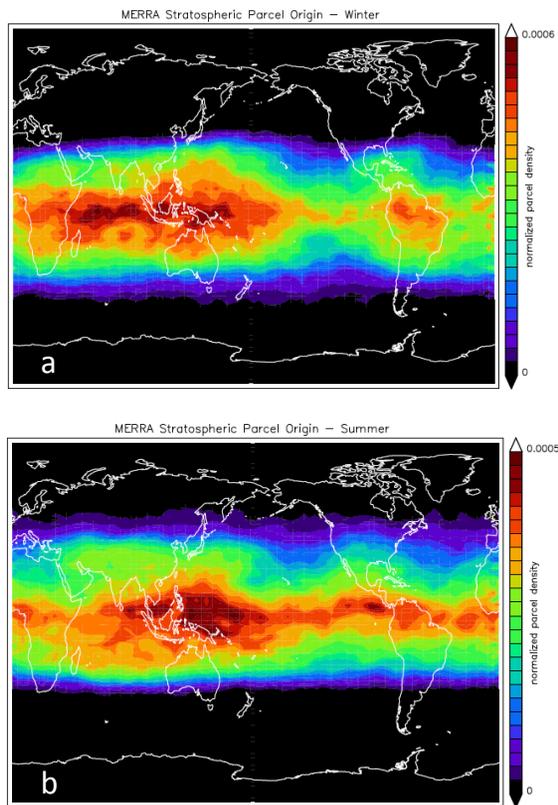
Fig. 8. Seasonal maps for TTL parcels that end up in the stratosphere (parcel origin). **(a)** Density map for 360 K parcels initiated during winter (DJF); **(b)** summer (JJA). The color scheme and color bars referenced as in Fig. 1.

Title Page

Abstract | Introduction

Conclusions | References

Tables | Figures

Back | Close

Full Screen / Esc

Printer-friendly Version

Interactive Discussion
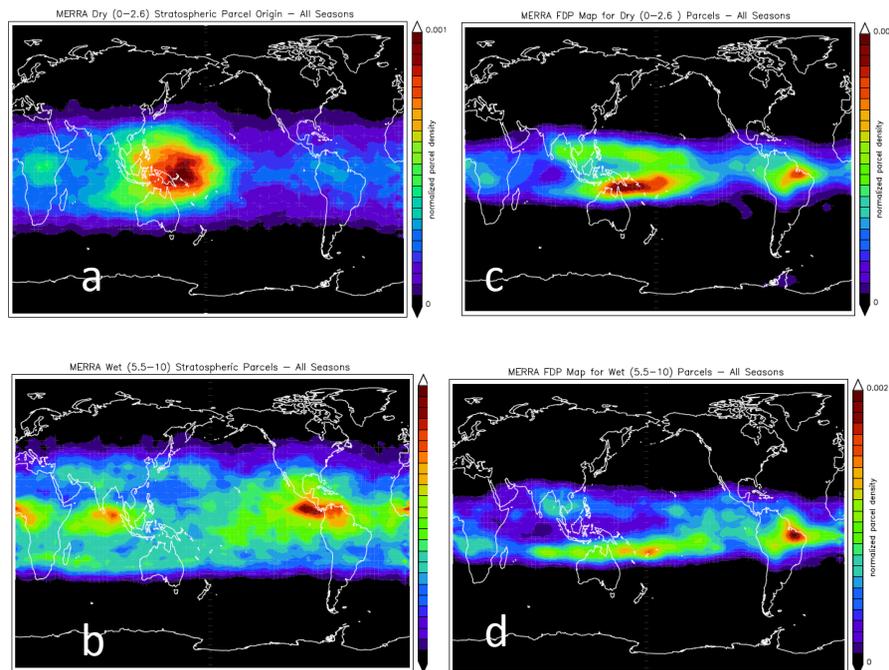
Fig. 9. 360 K parcel density maps of dry **(a)** and wet **(b)** parcels in the stratosphere and FDP density maps of the driest **(c)** and wettest **(d)** air. Wettest parcels (5.5–10 ppmv) are about 10 % of the total number of parcels; driest (0–2.6 ppmv) are about 14 %. The color scheme and color bars referenced as in Fig. 1.
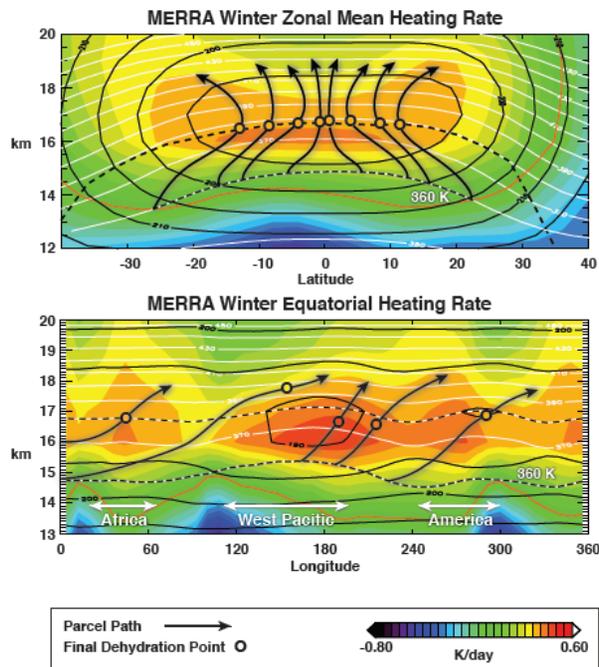
Fig. 10. Diagram of the dehydration process. Parcel paths are black arrows. The color background shows the heating rate from MERRA; black contours are temperature, and white contours are potential temperature. Thin dashed black line is the tropopause, thick dashed black line is 360 K surface – the level where parcels in our model are initialized. Top figure is zonal mean cross section where the air parcels moving upward concentrate latitudinally at the tropopause before rising into the stratosphere. Lower figure shows parcel paths vs. longitude along the equator. Small circles in both figures indicate the final dehydration points showing that the dehydration can take place at different altitudes. See text for details.